Electron Mean Free Path in a Spherical Shell Geometry

Alexander Moroz*

Wave-scattering.com

Received: February 2, 2008; Revised Manuscript Received: March 25, 2008

Mean free path is calculated for the shell geometry under the assumptions of (i) diffusive, (ii) isotropic, and (iii) billiard, or Lambertian, scattering. Whereas in a homogeneous sphere case the difference between different models of surface scattering is reflected merely by a different slope of the linear dependence of a mean free path $L_{\rm eff}$ on the sphere radius R, qualitatively different nonlinear dependencies on the inner and outer shell radii result for different model cases in the shell geometry. A linear behavior of $L_{\rm eff}$ on the shell thickness (D) can only be established for the billiard model in the thin shell limit, in which case $L_{\rm eff} \approx 2D$, whereas, in the same limit, $L_{\rm eff} \approx (D/2)\ln(2R/D)$ in the diffusive case and $L_{\rm eff} \approx 14(2RD)^{1/2}/[3\ln(2R/D)]$ in the isotropic case. The shell geometry turns out a very sensitive setup to distinguish between the different models of electron scattering, which could be performed in future experiments on single and well-controlled dielectric core-metal shell nanoparticles. This would enable one to more precisely assess the contribution of other mechanisms, such as chemical interface damping, to overall plasmon resonance damping. Preliminary experimental results are compatible with the billiard, or Lambertian, scattering model and appear to rule out both the Euler diffusive scattering and the isotropic scattering.

1. Introduction

Recently, a novel class of metallo-dielectric particles composed of a dielectric core and a metal shell, also called nanoshells, has gained a strong interest. These structures have the unique property that their surface plasmon frequency is extremely sensitive to the thickness of the metal shell.[1–5] Nanoshells offer significant advantages over conventional imaging probes, including continuous and broad wavelength tunability, far greater scattering and absorption coefficients, increased chemical stability, and improved biocompatibility. Becaus of their unique properties, the functionalized nanoshells have been proposed as photothermal converters in a range of applications including photothermal cancer therapy and photothermally triggered drug release.[6] Further applications involve the use of gold nanoshell bioconjugates for molecular imaging in living cells,[7] to improve single nanoparticle molecular sensors sensitivity[8] and as molecular imaging multilabels.[9]

However, a practical realization of the applications that makes use of the plasmon resonance, such as photothermal applications,[6] sensing,[8] and multilabel applications,[9] is strongly influenced by the line shape broadening.[10] As well-known from the case of homogeneous metallic particles,[11–18] the line shape of the plasmon resonance in small metallic particles is significantly affected by its size. Assuming quasicontinuous energy bands of electrons, that is, that the discrete quantum energy levels broadening exceeds the mean spacing between the levels, it is believed to be justified to apply a purely classical reasoning that the line shape broadening effect is essentially geometric in its origin.[11–14,17] The standard classical approach for describing the size dependence of the dielectric function assumes that if a particle size is comparable to or smaller than the mean free path of conduction electrons in the bulk material (l_∞),[12,13,19] then the scattering of the conduction electrons from the particle surface results in a reduced effective mean free path ($L_{\rm eff}$), and an increased homogeneous line width—the full width at half-maximum (fwhm)—of the dipole plasmon polariton (Γ), through the Mathiessen's rule[11–17]

$$\Gamma = \Gamma_0 + \frac{v_F}{L_{\rm eff}} \tag{1}$$

Here v_F is the Fermi velocity of conduction electrons, and $\Gamma_0 = v_F/l_\infty$ describes the intrinsic bulk width of the dipole plasmon polariton. The ratio $v_F/L_{\rm eff}$ may be classically interpreted as the effective rate of scattering of the conduction electrons off the particle surface. The line width Γ directly determines the dephasing time $T_2 = 2\hbar/\Gamma$, where $\hbar$ is Planck's constant, the quality factor (Q) of the resonance at an energy $E_{\rm res}$ via the formula $Q = E_{\rm res}/\Gamma$, and the local field enhancement factor $|f|$[20] (in a harmonic model $|f| = Q$).[21]

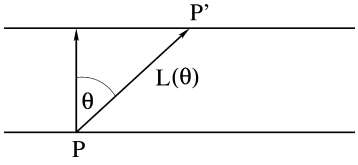

Figure 1. Definition of the parameters in a slab geometry. The chord length is $L(\theta) = D/\cos\theta$, where D is the slab thickness.

Surprisingly enough, and in striking contrast to the obvious practical importance of the nanoshell case, there is no agreement regarding the relevant $L_{\rm eff}$ in the spherical shell case. Contrary to a homogeneous sphere case (Appendix B), different approximate formulas are abundant in the literature for $L_{\rm eff}$ in the nanoshell case, often ad-hoc and not supported by any underlying model of surface scattering. In the case of thin shells, the most popular choice by far is to simply set $L_{\rm eff}$ equal to the shell thickness (D).[2–5,8] The usual reasoning is that, from the viewpoint of an electron, a thin shell is more comparable to a thin film than to a solid nanosphere. Yet, it is not difficult to show that the classical mean free path for a thin film diverges. Upon integrating the chord length $L(\theta) = D/\cos\theta$ over $\theta \in (0, \pi/2 - \delta)$ (Figure 1)

* E-mail: wavescattering@yahoo.com.

10.1021/jp8010074 CCC: $40.75
Published on Web 06/27/2008

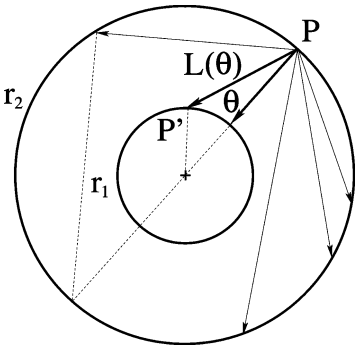

Figure 2. Spherical shell geometry and the definition of parameters for a point on the outer shell boundary. The chord length $L(\theta)$ is given by eq 7. Typical triangles used to calculate $L(\theta)$ are shown by dashed lines.

$$D\int_0^{\pi/2-\delta}\frac{\sin\theta\,\mathrm{d}\theta}{\cos\theta}=D\int_\delta^1\frac{\mathrm{d}x}{x}$$
$$=D\ln x|_\delta^1$$
$$=D\ln(1/\delta)\rightarrow\infty\quad(\delta\rightarrow 0)\qquad(2)$$

To support the classical arguments leading to the mean free path,

$$L_c=D\qquad(3)$$

one is thus forced to bail out by recalling seminal quantum-mechanical result for thin films. In the limit of $\hbar\omega \ll E_F$, with E_F and ω being the Fermi energy and frequency, respectively, the result is[22,23]

$$L_{QM}\approx\frac{2}{3}D\qquad(4)$$

Another popular choice is the Granqvist and Hunderi result.[24,25] Let r_1 and r_2 be the radii of the inner and outer surfaces of the shell, respectively. Then, when eq 6 of ref 24 is rewritten in terms of the radii, the Granqvist and Hunderi effective mean free path reads

$$L_{GH}=[(r_2-r_1)(r_2^2-r_1^2)]^{1/3}=D[2(r_2/D)-1]^{1/3}\qquad(5)$$

Equation 5 is sometime misquoted with a 1/2 prefactor,[26,27] and, in order to fit better experimental results, is additionally scaled by yet another 1/2 factor.[26,27] However, the Granqvist and Hunderi result (eq 5) is rather a rough estimate of the mean free path. To understand this expression, imagine a tangent to the inner sphere; the length along the tangent between the two spheres is, upon applying the Pythagorean theorem, $t=\sqrt{(r_2^2-r_1^2)}$. The formula is then equivalent to the cubic root of a believed to be characteristic volume element Dt^2, that is, $L_{GH}=(Dt^2)^{1/3}$.

Xu[28] took into account that there are electron trajectories within a shell that (i) connect the inner and the outer surface of the shell and that (ii) connect two points on the outer surface without cutting the inner shell surface. Let θ be the angle between the electron trajectory and the radius at the cross point on the outer shell surface (Figure 2). Then, the first set of trajectories occurs when $\sin\theta \le r_1/r_2$, whereas the second set of trajectories takes place when $\sin\theta > r_1/r_2$. The separation point between the two different sets of trajectories is given by

$$\sin\theta_c=r_1/r_2\qquad(6)$$

The corresponding lengths of the two set of trajectories as a function of θ are then

$$L(\theta)=\begin{cases}r_2\cos\theta-\sqrt{r_1^2-r_2^2\sin^2\theta}, & \theta\le\theta_c\\ 2r_2\cos\theta, & \theta>\theta_c\end{cases}\qquad(7)$$

The resulting mean free path is then given by

$$L_{Xu}=\int_0^{\pi/2}L(\theta)\sin\theta\,\mathrm{d}\theta\qquad(8)$$

However, the expression is largely incomplete, because the contribution of the points on the inner shell boundary to the mean free path has been entirely neglected.

Kachan and Ponyavina [31,32] suggested the following formula for the electron mean free path in a shell geometry:

$$L_{KP}=R\left[\frac{1}{1+q^2}-\frac{q}{2}-\frac{1}{4}\frac{(1-q^2)}{(1+q^2)}(1-q)\ln\frac{(1-q)}{(1+q)}\right]\qquad(9)$$

where $R=r_2$ and $q=r_1/r_2$. The formula has been employed by, for example, Boris and Nikolai Khlebtsov[10] and others.[21] However, the Kachan and Ponyavina result for mean free path is again unsatisfactory, because it does not correspond to any customary model assumptions about the surface scattering.

Eventually, in a seemingly unrelated field of billiards, a remarkably simple formula has been derived, which yields the mean free path entirely in terms of the geometrical parameters of a bounded and connected domain Q under consideration[29,30]

$$L_B=\frac{|Q|\cdot|S^{d-1}|}{|\partial Q|\cdot|B^{d-1}|}\qquad(10)$$

Here, $|Q|$ is the volume of Q, $|\partial Q|$ is the area of the surface ∂Q of Q, $|S^{d-1}|$ is the surface of a unit sphere in R^d, and $|B^{d-1}| = |S^{d-2}|/(d-1)$ is the volume of a unit ball in R^{d-1}. One has the following relations

$$S^1=2\pi,\ S^2=4\pi,\ B^1=2,\ B^2=\pi\qquad(11)$$

In particular, for planar billiards ($d=2$)

$$L_B=\frac{\pi|Q|}{|\partial Q|}\qquad(12)$$

whereas for three-dimensional billiards ($d=3$)

$$L_B=\frac{4|Q|}{|\partial Q|}\qquad(13)$$

Thus, in the present case of a spherical shell geometry,

$$L_B=\frac{4(r_2^3-r_1^3)}{3(r_2^2+r_1^2)}=\frac{4R}{3}\frac{1-q^3}{1+q^2}\qquad(14)$$

In the following, the mean free path for shell geometry will be calculated (i) on assuming Euler diffusive surface scattering[11] and (ii) under the assumption of a homogeneous and isotropic electron distribution within a shell. Further, the billiard formula (eq 14) in the nanoshell case will be confirmed by an explicit averaging procedure. It will be demonstrated that the very same result also follows upon assuming that the electron scattering events on the domain surface ∂Q conspire to produce a "Lambertian" surface (see Section 2.1). It will be shown that preliminary experimental results,[3–5,8,36] which were performed exclusively within the range $D/R \lesssim 0.25$, are compatible with the billiard, or Lambertian, scattering model and rule out both the Euler diffusive scattering and the isotropic scattering. The success of the Euler diffusive scattering in the homogeneous sphere case[11–14] seems to be purely accidental, since all the scattering models yield a linear dependence of the mean free path on the sphere radius with minor differences in the slope (see Appendix B). Contrary to the homogeneous sphere case,

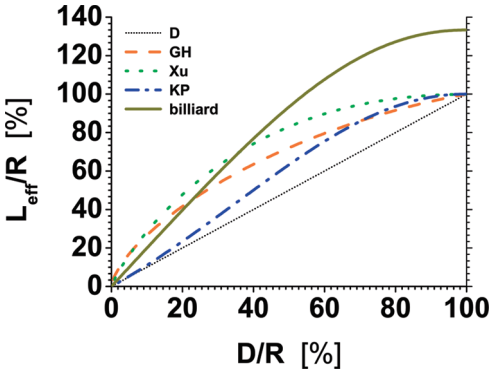

Figure 3. The mean free path in the spherical shell case for different surface scattering models as a function of the ratio D/R, where D is the shell thickness and R is the shell outer radius.

the mean free path in the shell geometry turns out to be much more sensitive to underlying model assumptions of electron surface scattering. Consequently, future experiments on single and well-controlled dielectric core-metal shell nanoparticles can much easier differentiate between competing models of surface scattering. The outline of the article is as follows. In Section 2 we review different models of surface scattering, summarize notation, and give some basic definitions. Section 3 deals with the mean free path for a diffusive scattering. The resulting mean free path is given by eq 47, or, in terms of R and q, by eq 71. As a byproduct, an explicit expression for L_{Xu} is obtained by performing the integral in eq 8 (see eqs 54 and 55). The billiard formula (eq 14) in the spherical shell case is confirmed in Section 4. The mean free path for an isotropic scattering is determined by eq 85 and is derived in Section 5. Section 6 summarizes asymptotic behavior for different models, both in the thin shell and in the vanishing core limits. In Section 7, the main properties of the billiard model are singled out. Comparison with experimental data is reviewed in Section 7.1. Theoretical and practical implications are summarized in Section 7.2. We then conclude by Section 8. Intermediary calculational steps together with the wording of the Birkhoff−Khinchin theorem and a derivation of the billiard formula in its general form (eq 10) are supplied as Supporting Information.

2. Notation and Definitions

At any point P of the boundary surface ∂Q of Q let us introduce the spherical coordinates with the origin at P and with the z-axis along the inward normal. Let $L(\theta, \varphi)$ be the length of the straight line PP' connecting the point P with an opposite boundary point P' at an angles (θ, φ) to the inward normal at P. The averaging over different chord lengths $L(\theta, \varphi)$ emanating from P will involve an integration over the solid angle of 2π-steradians above the tangent plane at the point P, that is, with the integration range $\theta \in (0, \pi/2)$, $\varphi \in (0, 2\pi)$, with a measure $d\mu(\theta, \varphi)$,

$$l_P = \int L(\theta,\ \varphi)\, d\mu(\theta,\ \varphi) \tag{15}$$

The resulting mean free path is then defined by

$$L_{\text{eff}} = \frac{\int_{\partial Q} l_P\, dS}{|\partial Q|} \tag{16}$$

2.1. Surface Scattering Models. ***Euler Model.*** Out of the various surface scattering models the Euler diffusive surface scattering model[11] is the oldest one. The model is concerned with the trajectories immediately after individual scattering events. The electron reflection on the boundary surface is taken to be fully isotropic, meaning there is equal probability for electrons to be scattered at any angle with respect to the surface normal. For that reason, the model is sometime referred to as the isotropic scattering model.[14−16] The resulting probability measure in the spherical coordinates with the origin at a given surface point is then

$$d\mu_d = c_d \sin\theta\, d\theta\, d\varphi \tag{17}$$

where the normalization factor

$$c_d^{-1} = \int_0^{\pi/2} \sin\theta\, d\theta \int_0^{2\pi} d\varphi = 2\pi \tag{18}$$

Isotropic Model. In contrast to the Euler model,[11] an isotropic scattering is concerned with the trajectories immediately before scattering events. No explicit assumption is made about individual scattering events at the enclosure boundary except that the scattering events conspire to maintain a homogeneous and isotropic particle distribution in the enclosure Q.[13] To find the corresponding measure for the chord lengths, the following gedanken experiment is performed. Assume that the enclosure boundary has been switch on instantaneously from its impermeable state to a fully permeable state. Let us now consider the amount of particles that will be detected by a detector located at a given enclosure boundary point P at a particular angle with respect to the inward normal to the enclosure boundary. Obviously, the number of detected particles will be proportional to $L(\theta, \varphi)$. Each particle arriving at an angle (θ, φ) to the detector then transversed the length $L(\theta, \varphi)$ from the latest collision at the boundary surface. This results in the following measure in the spherical coordinates,

$$d\mu_i = c_i L(\theta, \varphi) \sin\theta\, d\theta\, d\varphi \tag{19}$$

with the normalization factor

$$c_i^{-1} = \int_0^{\pi/2} \sin\theta\, d\theta \int_0^{2\pi} L(\theta, \varphi)\, d\varphi \tag{20}$$

Billiard Scattering Model. The billiard scattering model presumes a specular reflection at the enclosure boundary, that is, the angle of incidence equals the angle of reflection. This allows one to unambiguously follow any given electron trajectory. In contrast to previous models, further considerations in the billiard case follow in the phase space. The latter is $M = \bar{Q} \times S^{d-1}$, where $\bar{Q}$ is the closure of the domain Q, and S^{d-1} is the $(d - 1)$-dimensional unit sphere of all velocity vectors. What is eventually of the main importance is actually the "boundary" subspace M of the phase space $\mathbf{M}$, defined as

$$M := \{x = (\mathbf{s}, \mathbf{v}) \in \boldsymbol{M} : s \in \partial Q,\ \mathbf{v} \cdot \mathbf{n}(\mathbf{s}) \geq 0\} \tag{21}$$

Obviously, the configuration subspace of M is the boundary ∂Q of Q and velocity vectors $v \in M$ are all possible outgoing unit velocity vectors (note that the scalar product $\mathbf{v} \cdot \mathbf{n}$ of $\mathbf{v}$ with the inward normal $\mathbf{n}$ at $\mathbf{s} \in \partial Q$ is required to be positive) resulting from reflections at ∂Q. In brief, the subset M consists of all the points of the phase space $\mathbf{M}$ immediately after reflections at ∂Q.

Select a set of electrons immediately after their reflections at ∂Q. By the above definition, such a set forms a subset, call it A, of M. The electrons of the initial set A will continue their uniform straightforward motion, or a flow, until they reflect at ∂Q again, in which case the set $A \subset M$ will transform into a set $TA \subset M$, etc. These repeating transformations of the initial set A define a map, $T : A \rightarrow TA$, which is usually called the billiard map. After subsequent reflections at ∂Q, the initial set A is thus mapped into sets TA, T^2A, etc, and undergoes continuous

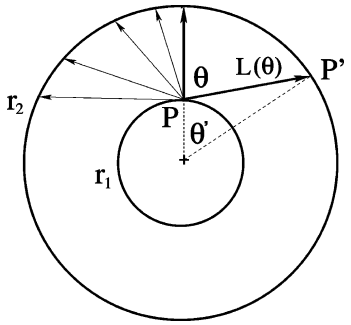

Figure 4. Spherical shell geometry and the definition of parameters for a point on the inner shell boundary. The chord length L in θ-coordinates is given by eq 36, and that in θ'-coordinates is given by eq 39. A triangle used to calculate the highlighted chord length L by the cosine formula (eq 122) in θ'-coordinates is shown by dashed lines.

changes in its underlying configuration and velocity subsets, which will spread or shrink depending on the geometry of ∂Q. Obviously, when focusing on either the configuration or velocity subset of A, the corresponding Lebesgue measure of such a subset will change after each collision. The billiard measure is the measure that is invariant under subsequent reflections of the initial set $A \subset M$ of electrons and yields the very same measure of the initial set A after any reflection. In other words,

$$\mu_B(A) = \mu_B(TA) = \mu_B(T^2A) = \ ... \ = \mu_B(T^nA) \tag{22}$$

The resulting invariant measure in the spherical coordinates is[29,30]

$$d\mu_B = c_B(\mathbf{v} \cdot \mathbf{n}) \sin\theta \, d\theta \, d\varphi = c_B \cos\theta \sin\theta \, d\theta \, d\varphi \tag{23}$$

with the normalization factor

$$c_B^{-1} = \int_0^{\pi/2} \cos\theta \sin\theta \, d\theta \int_0^{2\pi} d\varphi = |B^2| = \pi \tag{24}$$

Note the extra "cos θ" factor in the billiard measure[17] with regard to the Euler measure.[17] The "cos θ" factor is to compensate against the Jacobian of the transformation $T : A \rightarrow TA$. Indeed, one finds

$$|\det DT(x)| = \frac{\cos\theta}{\cos\theta_1} \tag{25}$$

where the θ and θ_1 are the angles of the unit velocity vectors of the phase space points x and Tx, respectively, with regard to the inward normal at the projections of x and Tx onto ∂Q (see pp 110−112, 116−118, and Figure IV.2 of ref 30). Hence, when the measure of TA is calculated by the substitution of variables with regard to the map $T : A \rightarrow TA$,

$$\mu_B(TA) = 2\int_{TA} \cos\theta_1 \, d\mathbf{s}_1 \, d\mathbf{v}_1 = 2\int_A \cos\theta_1 |\det DT(x)| \, d\mathbf{s} \, d\mathbf{v} = 2\int_A \cos\theta_1 \frac{\cos\theta}{\cos\theta_1} \, d\mathbf{s} \, d\mathbf{v} = \mu_B(A) \tag{26}$$

where $d\mathbf{v} = \sin\theta \, d\theta \, d\varphi$ is the Lebesgue measure on S^{d-1} for $d = 3$, and $d\mathbf{s}$ is the Lebesgue measure on ∂Q. Physically, the extra "cos θ" factor in the billiard measure[17] with regard to the Euler measure[17] can be interpreted as that the electron enclosure surface is a "Lambertian" surface. The latter is distinguished by a fact that the radiant intensity observed from it is directly proportional to the cosine of the angle θ between the observer's line of sight and the surface normal; hence, when an area element on the surface is viewed from any angle, it has the same radiance. (An example a perfect Lambertian radiator is a blackbody, and, to a large extent, the Sun in the visible spectrum.) Consequently, the billiard measure[17] can be interpreted as that the electron scattering events on the domain surface ∂Q conspire to produce a diffusive "Lambertian" surface. The condition of specular reflections can then be abandoned.

2.2. Shell Geometry—Summary of Basic Formulas. Shell geometry brings about several simplifications to the above general considerations. First, in virtue of the axial symmetry along the inward normal, the chord length $L(\theta, \varphi)$ emanating from any fixed P does not depend on φ, and the integration in eq 15 over φ is trivial. Therefore, one can replace eq 15 by

$$l_P = \int L(\theta) \, d\mu(\theta) \tag{27}$$

with the following reduced probability measures

$$d\mu_d(\theta) = \sin\theta \, d\theta \tag{28}$$

$$d\mu_i(\theta) = c_i L(\theta) \sin\theta \, d\theta \tag{29}$$

with the normalization factor c_i being the inverse of l_P in the diffusive case, wherein the normalization factor c_i is

$$c_i^{-1} = \int_0^{\pi/2} L(\theta) \sin\theta \, d\theta = l_{P;d} \tag{30}$$

and

$$d\mu_B(\theta) = 2\cos\theta \sin\theta \, d\theta \tag{31}$$

Second, because of the spherical symmetry, for all the points on the shell-ambient interface the very same average chord length $l_P = l_2$ is obtained after performing the integral in eq 27. Similarly, all the points on the shell−core interface are equivalent when the value of the integral in eq 27 is concerned; in this case the average chord length is denoted by l_1. Consequently, the surface integral in eq 16 is replaced by a simple algebraic relation. The formula for the resulting mean free path then simplifies from eq 16 to

$$L_{eff} = \frac{r_2^2 l_2 + r_1^2 l_1}{r_2^2 + r_1^2} \tag{32}$$

For a point on the outer shell boundary (Figure 2), that is, on the shell-ambient interface, the chord length $L(\theta)$ is given by eq 7. Upon substituting eq 7 into the integral in eq 27, three different integrals result,

$$S_1 = 2R\int_{\theta_c}^{\pi} \cos\theta \, d\mu(\theta) \tag{33}$$

$$S_2 = \int_0^{\theta_c} \sqrt{r_1^2 - r_2^2 \sin^2\theta} \, d\mu(\theta) \tag{34}$$

$$S_3 = R\int_0^{\theta_c} \cos\theta \, d\mu(\theta) \tag{35}$$

where, as usual, $R = r_2$ and the limit point θ_c in the above integrals is defined by eq 6.

For points on the inner shell boundary, or, on the shell−core interface, it turns out that the integral in eq 27 with the diffusive and billiard measures can be more easily performed in the spherical coordinates with the origin coinciding with the centers of the two concentric spheres forming the shell boundaries and with the z-axis oriented along the segment connecting the origin with the point P. In what follows, the spherical coordinates at the point P will be referred to as the θ-coordinates, and the latter coordinates as the θ'-coordinates. (See Figure 4 for θ and θ' definitions.) The chord length can be most easily found in the θ'-coordinates. Indeed, on applying the law of cosines (eq 122),

$$L(\theta') = [r_1^2 + r_2^2 - 2r_1 r_2 \cos\theta']^{1/2} \tag{36}$$

Note that the angle θ' is limited within the interval for which $\cos\theta' \in (1, r_1/r_2)$, that is, $\theta' \in (0, \theta'_m)$, where

$$\cos\theta'_m = r_1/r_2 \tag{37}$$

On using

$$\sin\theta = \frac{r_2}{L}\sin\theta' \tag{38}$$

expressing $\cos\theta'$ in eq 36 in terms of $\sin\theta$, and upon solving a quadratic equation for L^2, one arrives at the chord length in the θ-coordinates:

$$L^2(\theta) = (r_1^2 + r_2^2) - 2r_1^2\sin^2\theta - 2r_1\cos\theta\sqrt{r_2^2 - r_1^2\sin^2\theta} \tag{39}$$

where $\theta \in (0, \pi/2)$. In what follows, it turns out expedient to introduce a shorthand

$$\beta = \frac{r_1^2 + r_2^2}{2r_1 r_2} \tag{40}$$

β can be shown to satisfy the following straightforward relations

$$\beta \pm 1 = \frac{(r_2 \pm r_1)^2}{2r_1 r_2} \tag{41}$$

$$\beta - (r_1/r_2) = \frac{r_2^2 - r_1^2}{2r_1 r_2} \tag{42}$$

$$\beta^2 - 1 = \frac{(r_2^2 - r_1^2)^2}{(2r_1 r_2)^2} \tag{43}$$

To this end, we recast $L(\theta')$ in eq 36 in terms of $x = \cos\theta'$ and β

$$L(\theta') = \sqrt{2r_1 r_2}(\beta - x)^{1/2} \tag{44}$$

In what follows, the following two formulas will be repeatedly used:

$$\cos\theta\, d\theta = \frac{r_2}{\sqrt{2r_1 r_2}}\frac{d\theta'}{(\beta - x)^{1/2}}\left[x - \frac{1}{2(\beta - x)} + \frac{x^2}{2(\beta - x)}\right] \tag{45}$$

$$d\theta = \frac{d\theta'}{x - (r_1/r_2)}\left[x - \frac{1}{2(\beta - x)} + \frac{x^2}{2(\beta - x)}\right] \tag{46}$$

3. Diffusive Scattering

In this section, the following expression for the resulting mean free path for a diffusive scattering in the shell geometry will be derived:

$$L_d = \frac{1}{4(r_1^2 + r_2^2)}\left[4r_2^3 - 2r_1(r_1^2 + r_2^2) - (r_2 + r_1)^2(r_2 - r_1)\ln\left(\frac{r_2 - r_1}{r_2 + r_1}\right)\right] \tag{47}$$

(Its equivalent form in terms of R and q is given as eq 71 below.)

3.1. A Point Located on the Outer Shell Boundary. The task in the present case amounts to the calculation of the Xu mean free path L_{Xu} as given by eq 8, with $L(\theta)$ given by eq 7. The respective integrals in eqs 33 and 35 with the measure $d\mu_d$ can be performed on using eq 123,

$$S_1 = 2r_2\int_{\theta_c}^{\pi/2}\cos\theta\sin\theta\, d\theta = r_2[1 - (r_1/r_2)^2] \tag{48}$$

$$S_3 = r_2\int_0^{\theta_c}\cos\theta\sin\theta\, d\theta = \frac{r_2}{2}(r_1/r_2)^2 \tag{49}$$

In arriving at the results in eqs 48 and 49, we have used the relation

$$\cos 2\theta_c = 1 - 2\sin^2\theta_c = 1 - 2(r_1/r_2)^2 \tag{50}$$

Next, the integral (eq 34) is recast as

$$S_2 = \int_0^{\theta_c}\sqrt{r_2^1 - r_2^2\sin^2\theta}\sin\theta\, d\theta = \int_1^a\sqrt{y^2 - 1}\, dy \tag{51}$$

where $x = \cos\theta$ and $y = ax$ with

$$a = \frac{1}{\sqrt{1 - (r_1/r_2)^2}} = \frac{1}{\cos\theta_c} \tag{52}$$

Here, the last equality follows upon using eq 6. Upon using the quadrature formula (eq 125),

$$S_2 = \frac{r_1}{2} + \frac{r_2}{4}[1 - (r_1/r_2)^2]\ln\frac{1 - (r_1/r_2)}{1 + (r_1/r_2)} \tag{53}$$

Eventually,

$$l_2 \equiv L_{Xu} = S_1 + S_3 - S_2 = \frac{r_2 - r_1}{2r_2}(2r_2 + r_1) - \frac{r_2^2 - r_1^2}{4r_2}\ln\left(\frac{r_2 - r_1}{r_2 + r_1}\right) \tag{54}$$

The above expression can be recast upon using the identity in eq 134 in terms of R and D as follows:

$$l_2 = \frac{D}{2}(2 + q) + R\frac{1 - q^2}{4}\ln\left(\frac{2R}{D} - 1\right) \tag{55}$$

We recall that the two equivalent expressions 54 and 55 are the explicit expressions of the Xu mean free path L_{Xu} as defined by eq 8.

Note in passing the respective asymptotic behaviors of l_2 in the thin shell and in the vanishing core limits. In the limit $r_1 \to r_2$, one finds eq 56, upon using the identities 135 and 136 in:

$$l_2 = \frac{D}{2}\left(3 - \frac{D}{R}\right) + \frac{D}{2}\ln\left(\frac{2R}{D} - 1\right) \approx \frac{D}{2}\ln\left(\frac{2R}{D} - 1\right) + \frac{3D}{2} \tag{56}$$

On the other hand, in the limit $r_1 \to 0$, eq 57 is obtained,

$$\ln\left(\frac{r_2 - r_1}{r_2 + r_1}\right) \approx -2r_1/r_2 + O[(r_1/r_2)^3] \tag{57}$$

and hence

$$l_2 \approx R\left(1 - \frac{q^2}{2}\right) \to R \quad (r_1 \to 0) \tag{58}$$

As expected, the Euler result[11] for a homogeneous sphere is recovered in the limit $r_1 \to 0$ (see eq 140 of Appendix B).

3.2. A Point Located on the Inner Shell Boundary. In the present case, the integral in eq 27 is most easily performed in the θ'-coordinates. Upon consecutively using eqs 38 and 46, the relation shown in eq 59 is obtained.

$$L\sin\theta\,\mathrm{d}\theta = r_2\sin\theta'\,\mathrm{d}\theta = -\frac{r_2\,\mathrm{d}x}{x-(r_1/r_2)}\left[x-\frac{1}{2(\beta-x)}+\frac{x^2}{2(\beta-x)}\right] \tag{59}$$

On taking into account

$$\int_0^{\theta'_{\mathrm{m}}} F(\cos\theta')\sin\theta'\,\mathrm{d}\theta' = -\int_1^{r_1/r_2} F(x)\,\mathrm{d}x = \int_{r_1/r_2}^1 F(x)\,\mathrm{d}x \tag{60}$$

$$l_1 = \int_0^{\pi/2} L(\theta)\sin\theta\,\mathrm{d}\theta = C_1 - C_2 + C_3 \tag{61}$$

where

$$C_1 = r_2\int_{r_1/r_2}^1 \frac{x\,\mathrm{d}x}{x-(r_1/r_2)} = \{r_2x + r_1\ln[x-(r_1/r_2)]\}\Big|_{r_1/r_2}^1 \tag{62}$$

$$C_2 = \frac{r_2}{2}\int_{r_1/r_2}^1 \frac{\mathrm{d}x}{[x-(r_1/r_2)](\beta-x)} = \frac{r_1r_2^2}{r_2^2-r_1^2}\{\ln[x-(r_1/r_2)] - \ln(\beta-x)\}\Big|_{r_1/r_2}^1 \tag{63}$$

and

$$C_3 = \frac{r_2}{2}\int_{r_1/r_2}^1 \frac{x^2\,\mathrm{d}x}{[x-(r_1/r_2)](\beta-x)} = -\frac{r_2}{2}\left\{x + \frac{2r_1r_2}{r_2^2-r_1^2}\{\beta^2\ln(\beta-x) - (r_1/r_2)^2\ln[x-(r_1/r_2)]\}\right\}\Bigg|_{r_1/r_2}^1 \tag{64}$$

Here, the integral C_1 has been performed on using the quadrature formula 126. The integral C_2 has been performed on using the quadrature formula 127, and taking into account that, within the integration range,

$$x \ge r_1/r_2, \quad x \le 1 \le \beta = \frac{r_1^2+r_2^2}{2r_1r_2} \tag{65}$$

Lastly, the integral C_3 has been performed on using the quadrature formula 128.

Let focus now in the above expressions for C_1, C_2, and C_3 on the terms proportional to the factor $\ln[x-(r_1/r_2)]$, which are divergent for $x = r_1/r_2$. Since

$$r_1 - \frac{r_1r_2^2}{r_2^2-r_1^2} + \frac{r_1^3}{r_2^2-r_1^2} \equiv 0 \tag{66}$$

the prefactors of terms proportional to the factor $\ln[x-(r_1/r_2)]$ simultaneously cancel out in the sum. Subsequently, after making use of the relations 41–43,

$$l_1 = C_1 - C_2 + C_3 = \left\{\frac{r_2x}{2} + \frac{r_1r_2^2}{r_2^2-r_1^2}(1-\beta^2)\ln(\beta-x)\right\}\Bigg|_{r_1/r_2}^1 = \frac{r_2-r_1}{2} - \frac{r_2^2-r_1^2}{4r_1}\ln\left(\frac{r_2-r_1}{r_2+r_1}\right) \tag{67}$$

For completeness, upon applying expressions 134–136 and 138 in eq 67, one finds in the limit $r_1 \to r_2$,

$$l_1 \approx \frac{D}{2}\ln\left(\frac{2R}{D}-1\right) + \frac{D}{2} \tag{68}$$

On using the asymptotic 57, one finds in the limit $r_1 \to 0$

$$l_1 \approx \frac{r_2-r_1}{2} + \frac{r_2+r_1}{2r_2}(r_2-r_1) \approx R\left(1-\frac{q}{2}\right) \tag{69}$$

3.3. Final Result. On substituting the partial results 54 and 67 into eq 32, one arrives at

$$L_d = \frac{r_2^2l_2 + r_1^2l_1}{r_2^2+r_1^2} = \frac{1}{4(r_1^2+r_2^2)}\left[4r_2^3 - 2r_1(r_1^2+r_2^2) - (r_2+r_1)(r_2^2-r_1^2)\ln\left(\frac{r_2-r_1}{r_2+r_1}\right)\right] \tag{70}$$

which proves the final result (eq 47). In terms of $R = r_2$ and $q = r_1/r_2$, the above expression can be recast as

$$L_{\mathrm{d}} = R\left[\frac{1}{1+q^2} - \frac{q}{2} - \frac{1}{4}\frac{(1-q^2)}{(1+q^2)}(1+q)\ln\frac{(1-q)}{(1+q)}\right] \tag{71}$$

This expression for the mean free path closely resembles eq 9 suggested by Kachan and Ponyavina; [31,32] the only difference is that the prefactor $(1-q)$ in front of the natural logarithm has been replaced by $(1+q)$ in the diffusive case. As shown in Section 6, this difference results, among other, in a qualitatively different asymptotic behavior in the thin-shell limit.

4. Billiard Scattering

In this section the general billiard formula (eq 14) will be confirmed by an explicit averaging according to eqs 15 and 32 with the reduced probability measure $\mathrm{d}\mu_{\mathrm{B}}$ (eq 31).

4.1. A Point Located on the Outer Shell Boundary. On performing the respective integrals in eqs 33–35 with the probability measure $\mathrm{d}\mu_{\mathrm{B}}$ (eq 31) one finds

$$S_1 = 4R\int_{\theta_{\mathrm{c}}}^{\pi/2}\cos^2\theta\sin\theta\,\mathrm{d}\theta = \frac{4R}{3}(1-q^2)^{3/2} \tag{72}$$

$$S_3 = 2R\int_0^{\theta_{\mathrm{c}}}\cos^2\theta\sin\theta\,\mathrm{d}\theta = \frac{2R}{3}[1-(1-q^2)^{3/2}] \tag{73}$$

$$S_2 = 2\int_0^{\theta_{\mathrm{c}}}\sqrt{r_1^2-r_1^2\sin^2\theta}\cos\theta\sin\theta\,\mathrm{d}\theta = \frac{\sqrt{r_2^2-r_1^2}}{2}\int_{\cos 2\theta_{\mathrm{c}}}^1\sqrt{ax-b}\,\mathrm{d}x \tag{74}$$

where $x = \cos 2\theta$ and

$$a = \frac{1}{2[1-(r_1/r_2)^2]}, \quad b = a\cos(2\theta_{\mathrm{c}}) \tag{75}$$

Hence

$$S_2 = \frac{\sqrt{r_2^2-r_1^2}}{3a}(ax-b)^{3/2}\Big|_{\cos 2\theta_{\mathrm{c}}}^1 = \frac{2r_2}{3}(r_1/r_2)^3 \tag{76}$$

Thus, the mean free path in a billiard measure for a point located on the outer shell boundary is

$$l_2 = S_1 + S_3 - S_2 = \frac{2r_2}{3}\{1-(r_1/r_2)^3 + [1-(r_1/r_2)^2]^{3/2}\} \tag{77}$$

Obviously, $l_2 \to 4R/3$ as $r_1 \to 0$, which is the billiard mean free

path for a homogeneous sphere (see eq 141 of Appendix B).

4.2. A Point Located on the Inner Shell Boundary. Upon consecutively using eqs 38 and 45,

$$2L\cos\theta\sin\theta\,\mathrm{d}\theta = 2r_2\cos\theta\sin\theta'\,\mathrm{d}\theta = -\frac{2r_2^2}{\sqrt{2r_1r_2}}\frac{dx}{(\beta-x)^{1/2}}\left[x-\frac{1}{2(\beta-x)}+\frac{x^2}{2(\beta-x)}\right] \quad (78)$$

On taking into account eq 60,

$$l_1 = 2\int_0^{\pi/2} L(\theta)\cos\theta\sin\theta\,\mathrm{d}\theta = C_1 - C_2 + C_3 \quad (79)$$

where

$$C_1 = \frac{2r_2^2}{\sqrt{2r_1r_2}}\int_{r_1/r_2}^1 \frac{x\,\mathrm{d}x}{(\beta-x)^{1/2}} = -\frac{4r_2^2}{3\sqrt{2r_1r_2}}(2\beta+x)(\beta-x)^{1/2}\Big|_{r_1/r_2}^1 \quad (80)$$

$$C_2 = \frac{r_2^2}{\sqrt{2r_1r_2}}\int_{r_1/r_2}^1 \frac{\mathrm{d}x}{(\beta-x)^{3/2}} = \frac{2r_2^2}{\sqrt{2r_1r_2}}\frac{1}{(\beta-x)^{1/2}}\Big|_{r_1/r_2}^1 \quad (81)$$

and

$$C_3 = \frac{r_2^2}{\sqrt{2r_1r_2}}\int_{r_1/r_2}^1 \frac{x^2dx}{(\beta-x)^{3/2}} = \frac{2r_2^2}{\sqrt{2r_1r_2}}\left\{-\frac{1}{3}(\beta-x)^{3/2}+2\beta(\beta-x)^{1/2}+\frac{\beta^2}{(\beta-x)^{1/2}}\right\}\Big|_{r_1/r_2}^1 \quad (82)$$

Here, the integral C_1 has been performed on using the quadrature formula 129. The integral C_2 has been performed upon using the quadrature formula 130, and taking into account that the inequalities of eq 65 hold within the integration range. Lastly, the integral C_3 has been performed on using the quadrature formula 131.

Upon combining partial results 80–82 and upon using eqs 41–43, one finds

$$l_1 = C_1 + C_2 + C_3 = \frac{r_2^2}{\sqrt{2r_1r_2}}\frac{1}{\sqrt{\beta-x}}\left[\frac{(\beta-x)^2}{3}+\beta^2-1\right]\Big|_{r_1/r_2}^1 = \frac{2r_2^2}{3r_1^2}\{1-(r_1/r_2)^3-[1-(r_1/r_2)^2]^{3/2}\} \quad (83)$$

Note that $l_1 \to R$ as $r_1 \to 0$.

4.3. Final Result. Upon combining eqs 77 and 83,

$$r_2^2l_2 + r_1^2l_1 = \frac{4r_2^3}{3}[1-(r_1/r_2)^3] = \frac{4}{3}(r_2^3-r_1^3) \quad (84)$$

The billiard formula (eq 14) for the resulting mean free path L_B is now straightforwardly recovered upon substituting the partial result (eq 84) into the averaging formula (eq 32).

5. Isotropic Scattering

The resulting mean free path in the isotropic case is rather cumbersome and, in line with eq 32, it will be written merely as

$$L_i = \frac{r_2^2l_2 + r_1^2l_1}{r_2^2+r_1^2} \quad (85)$$

where l_2 and l_1 are given by eqs 94 and 103, respectively, derived herein below.

5.1. A Point Located on the Outer Shell Boundary. For a point located on the outer shell boundary, the chord length is given by eq 7. The latter implies for $\theta \le \theta_c$

$$L^2(\theta) = 2r_2^2\cos^2\theta - (r_2^2-r_1^2) - 2r_2\cos\theta\sqrt{r_2^2\cos^2\theta-(r_2^2-r_1^2)} \quad (86)$$

and

$$L^2(\theta) = 4r_2^2\cos^2\theta \quad (87)$$

for $\theta > \theta_c$. Now, let

$$I = \int_0^{\pi/2} L^2(\theta)\sin\theta\,\mathrm{d}\theta = I_1 + I_2 + I_3 + I_4 \quad (88)$$

where, upon using eq 124,

$$I_1 = 4r_2^2\int_{\theta_c}^{\pi/2}\cos^2\theta\sin\theta\,\mathrm{d}\theta = \frac{4r_2^2}{3}[1-(r_1/r_2)^2]^{3/2} \quad (89)$$

$$I_2 = 2r_2^2\int_0^{\theta_c}\cos^2\theta\sin\theta\,\mathrm{d}\theta = \frac{2r_2^2}{3}\{1-[1-(r_1/r_2)^2]^{3/2}\} \quad (90)$$

$$I_3 = -(r_2^2-r_1^2)\int_0^{\theta_c}\sin\theta\,\mathrm{d}\theta = -(r_2^2-r_1^2)\{1-[1-(r_1/r_2)^2]^{1/2}\} \quad (91)$$

and, upon the substitution $y = \cos^2\theta$,

$$I_4 = -2r_2\int_0^{\theta_c}\mathrm{d}\theta\sin\theta\cos\theta\sqrt{r_2^2\cos^2\theta-(r_2^2-r_1^2)} = -r_2\int_{\cos^2\theta_c}^1 \mathrm{d}y\sqrt{r_2^2y-(r_2^2-r_1^2)} = -\frac{2r_1^3}{3r_2} \quad (92)$$

Thus

$$I = I_1 + I_2 + I_3 + I_4 = \frac{5r_2^2}{3}[1-(r_1/r_2)^2]^{3/2} - \frac{2r_1+r_2}{3r_2}(r_2-r_1)^2 \quad (93)$$

The resulting l_2 is then recovered as the ratio

$$l_2 = \frac{I}{l_{2;\mathrm{d}}} \quad (94)$$

where $l_{2;\mathrm{d}}$ is the diffusive l_2 given by eq 54.

Regarding behavior in the $r_1 \to r_2$ limit, the expression 93 can be recast upon writing $r_1 = R - D$ and upon using eqs 135 and 136 as

$$I = \frac{5R^2}{3}(1-q^2)^{3/2} - \frac{1+2q}{3}D^2 = \frac{10}{3}(2R)^{1/2}D^{3/2} - D^2 + O(D^{5/2}) \quad (95)$$

Hence, upon combining the above asymptotic with eq 56 [cf., an equivalent form, eq 109 below] in the diffusive case,

$$l_2 \sim \frac{20}{3}(2RD)^{1/2}\left[3+\ln\left(\frac{2R}{D}-1\right)\right]^{-1} \quad (96)$$

5.2. A Point Located on the Inner Shell Boundary. First, eq 39 is recast as

$$L^2(\theta) = (r_1^2 + r_2^2) - 2r_1^2(1 - \cos^2\theta) - 2r_1\cos\theta\sqrt{r_2^2 - r_1^2 + r_1^2\cos^2\theta} \quad (97)$$

On performing the integral

$$I = \int_0^{\pi/2} L^2 \sin\theta \, d\theta \quad (98)$$

the three terms on the right-hand side of expression 97 give rise to three different integrals that will be separately treated. Thus $I = I_1 + I_2 + I_3$, where

$$I_1 = (r_1^2 + r_2^2)\int_0^{\pi/2} \sin\theta \, d\theta = r_1^2 + r_2^2 \quad (99)$$

$$I_2 = -2r_1^2\int_0^{\pi/2} (1 - \cos^2\theta)\sin\theta \, d\theta = -\frac{4r_1^2}{3} \quad (100)$$

and, upon the substitution $y = \cos^2\theta$,

$$I_3 = -2r_1\int_0^{\pi/2} \sqrt{r_2^2 - r_1^2 + r_1^2\cos^2\theta}\cos\theta\sin\theta \, d\theta = -r_1\int_0^1 dy\sqrt{r_2^2 - r_1^2 + r_1^2 y} = -\frac{2r_2^3}{3r_1}\{1 - [1 - (r_1/r_2)^2]^{3/2}\} \quad (101)$$

On combining the partial results together,

$$I = I_1 + I_2 + I_3 = \frac{2r_2^3}{3r_1}[1 - (r_1/r_2)^2]^{3/2} - \frac{2r_2 + r_1}{3r_1}(r_2 - r_1)^2 \quad (102)$$

The resulting l_1 is then recovered as the ratio

$$l_1 = \frac{I}{l_{1;d}} \quad (103)$$

where $l_{1;d}$ is the diffusive l_1 given by eq 67.

Regarding behavior in the $r_1 \to r_2$ limit, eq 102 can be recast upon using the identities 136 and 138 as

$$I \approx \frac{4}{3}(2R)^{1/2}D^{3/2} - \frac{2}{3}D^2 \quad (104)$$

Upon combining the above leading term of the asymptotic with that of eq 68,

$$l_1 \approx \frac{8}{3}(2RD)^{1/2}\left[1 + \ln\left(\frac{2R}{D} - 1\right)\right]^{-1} \quad (D \to 0) \quad (105)$$

Regarding behavior in the $r_1 \to 0$ limit,

$$I \approx \frac{2r_2^3}{3r_1}\{[1 - (r_1/r_2)^2]^{3/2} - [1 - (r_1/r_2)]^2\} - \frac{r_2^2}{3}[1 - (r_1/r_2)]^2 \approx R^2\left(\frac{4}{3} - \frac{1}{3}\right) + \frac{1}{3}R^2 q(-5 + 2) \approx R^2(1 - q) \quad (106)$$

Eventually, upon combining the above asymptotic with that of eq 69,

$$l_1 \approx R(1 - q)\left(1 - \frac{q}{2}\right)^{-1} \approx R - \frac{Rq}{2} \quad (r_1 \to 0) \quad (107)$$

6. Asymptotic Behavior

In the vanishing core limit $r_1 \to 0$ one recovers the homogeneous sphere case results of Appendix B. In the limit $r_1 \to 0$, each of L_{GH}, L_{KP}, L_{Xu}, and L_d tends to R, whereas both L_B and L_i tend to $4R/3$.

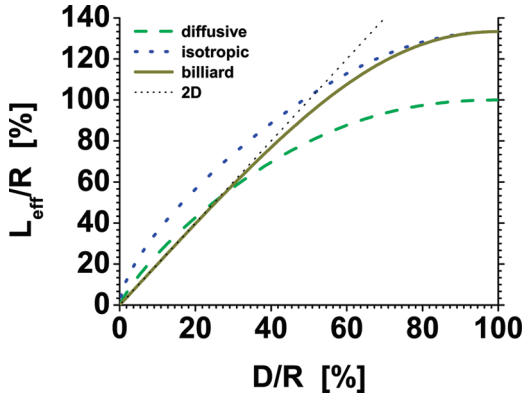

Figure 5. The mean free path in the spherical shell case for basic surface scattering models as a function of the ratio D/R, where D is the shell thickness and R is the shell outer radius. Coincidentally, all the experiments on size-dependent line width broadening in nanoshells [3–5,8,36] appear to be performed within the "linear" range $D/R \lesssim 0.25$.

Regarding asymptotic behavior in the thin shell limit, in a marked contrast to eq 3, the asymptotic of L_{GH} is no longer linear in the shell thickness D. Starting from eq 5 and upon using eq 134 one finds

$$L_{GH} = (2R - D)^{1/3}D^{2/3} \approx (2R)^{1/3}D^{2/3} \quad (D \to 0) \quad (108)$$

The asymptotic of L_{Xu} is that of l_2 as given by eq 56,

$$L_{Xu} \approx \frac{D}{2}\ln\left(\frac{2R}{D} - 1\right) + \frac{3D}{2} \quad (D \to 0) \quad (109)$$

The asymptotic of L_{KP} turns out to be linear in the shell thickness D. Indeed, upon employing eqs 135–137 in eq 9, one arrives at

$$L_{KP} \approx D + \frac{D^2}{4R}\ln\left(\frac{2R}{D} - 1\right) \quad (D \to 0) \quad (110)$$

Upon applying identities 135–137 in eq 71, one finds in the diffusive case:

$$L_d \approx \frac{D}{2}\ln\left(\frac{2R}{D} - 1\right) + D \quad (D \to 0) \quad (111)$$

On using eqs 135 and 137 in eq 14

$$L_B = \frac{4R}{3}\frac{1 - q^3}{1 + q^2} \quad (112)$$

one finds

$$L_B \approx \frac{4R}{3}\frac{3D}{2R}\left(1 - \frac{D}{R} + \frac{D^2}{3R^2}\right)\left(1 + \frac{D}{R} + \frac{D^2}{2R^2}\right) \approx 2D - \frac{D^3}{3R^2} \quad (D \to 0) \quad (113)$$

Note the absence of a $O(D^2)$ term in the asymptotic that results in a linear-like behavior of L_B over an extended range of shell thicknesses of up to $D/R \lesssim 0.3$ (Figure 5). Note also that the thin-shell asymptotic behavior of L_B in the shell geometry coincides with that for the slab geometry, provided that the integral in eq 2 is performed with a billiard measure (eq 31). Indeed, the following finite result is obtained in the latter case:

$$l = 2D\int_0^{\pi/2-\delta} \sin\theta \, d\theta = 2D\int_\delta^1 dx \to 2D \quad (\delta \to 0) \quad (114)$$

Given eqs 96 and 105, one finds in the isotropic case upon applying eq 85

$$L_i \approx \frac{14}{3}(2RD)^{1/2}\left[3+\ln\left(\frac{2R}{D}-1\right)\right]^{-1} \quad (D\rightarrow 0) \quad (115)$$

The leading order of some of the asymptotics could have been simplified. However, it has been found that by, for example, not neglecting 1 against $2R/D$ in the logarithm, the resulting asymptotics yield a good approximation to L_{Xu}, L_d, and L_i in a significantly larger parameter range.

7. Discussion

A common practice, derived from the homogeneous sphere case, that the mean free path in the shell geometry is proportional to the shell thickness and that different scattering models only affect the slope of this linear dependence[2–5,8] has been demonstrated to be invalid in the spherical shell case. Among the various models of surface scattering, the billiard, or Lambertian, model seems to be the most convincing from both purely theoretical and in view of explaining experimental data. Let us highlight the following features of the billiard, or Lambertian, surface scattering model:

(1) It is the only model that yields a linear behavior of the mean free path L_{eff} on the shell thickness D in the thin shell limit (up to $D/R \approx 0.3$; see Figure 5). Compare that with $L_d \approx (D/2)\ln(R/D)$ in the diffusive case, and with $L_i \approx 14(2RD)^{1/2}/[3 \ln (R/D)]$ in the isotropic case (see Section 6 for further details).

(2) For any shape of a bounded and connected electron enclosure Q and in any space dimension, the mean free path is straightforwardly determined by substituting the surface and volume of Q into eq 10.

(3) The billiard measure (eq 31) is the only measure that yields a finite result when the integral in eq 2 for the slab geometry is performed (see eq 114). It goes without saying that the result coincides with the thin-shell limit in the spherical shell geometry.

(4) Upon using the Birkhoff−Khinchin theorem, the billiard mean free path can be interpreted as the time average of the free paths along typical trajectories.

(5) It appears to agree with quantum-mechanical calculations.

(6) It gives the best agreement with the experimental data (see Section 7.1 below).

Regarding the second feature, in the special case of an arbitrary shape homogeneous convex particle, the geometric formula 10 has been rederived by Coronado and Schatz[33] using a geometrical probability approach, by imposing the condition that the resulting probability measure function, on set of all the lines, be invariant under rotation and translation of the three Cartesian coordinates x, y, and z. However, this approach cannot be used in the present case, because the spherical shell is not of a convex shape.

The third feature can be straightforwardly checked (see eqs 2 and 114). The fourth feature is about that the mean free path is not a simple average over path lengths. Time aspect is important as well. The mean free path is rather the time average of the free path along typical trajectories. The Birkhoff ergodic theorem (see ref 30 and Supporting Information) implies for $\tau(x) = L(x)/v_p$, with v_p being the particle velocity, that for almost every $x \in M$ the limit

$$\lim_{N\rightarrow\infty}\frac{1}{N}[L(x)+ \ldots + L(T^{N-2}x)+L(T^{N-1}x)] = \tilde{l}(x) \quad (116)$$

exists. The mean free path L_{eff} is then obtained by averaging $l(x)$ with respect to the probability measure $d\mu_B$ on M,

$$L_{eff} = \int \tilde{l}(x)\, d\mu_B = \int l(x)\, d\mu_B \quad (117)$$

Regarding the fifth feature, the billiard result (eq 141) results in the homogeneous sphere case[34] when original quantum mechanical calculation of the dielectric function on using linear response theory for a hard sphere model of noninteracting electrons in an infinitely deep spherical potential well by Kawabata and Kubo[35] are refined (see also ref 33 for further references). The only quantum-mechanical calculation in the spherical shell case has been performed by Kraus and Schatz,[18] who were able to manage the limiting case of thin shells (see Appendix 3 in ref 18), and who arrived at eq 118 (see Table 1 of ref 18)

$$L_{eff} = 2(\pi/3)^{1/3}D \approx 2.0309D \quad (118)$$

It goes without saying that the quantum-mechanical result almost exactly coincides with the billiard model thin-shell asymptotic (eq 113). However, the latter result has to be taken with caution, as the agreement with the classical asymptotic may be coincidental, because a refined Debye asymptotic expansions for large-order Bessel functions were not employed.

7.1 Comparison with Experiment. When measurements are performed on ensembles of fine metallic particles, the mean free path L_{eff} is typically determined from the size dependence of the imaginary part ε_2 of the dielectric constant,[13]

$$\varepsilon_2(\omega, R) = \varepsilon_{2b}(\omega) + \frac{\omega_p^2}{\omega^3}\frac{v_F}{L_{eff}} \quad (119)$$

where ε_{2b} is the size-independent bulk value, and ω_p is the plasma frequency. As a rule, the imaginary part of the dielectric constant is derived by Kramers−Kronig analysis from the measured absorption spectra. In Figure 7 of ref 13, Kreibig compared the predictions of the diffusive and isotropic models in the homogeneous sphere case against experimental data. [The Kawabata and Kubo quantum-mechanical prediction (labeled as KK line) has already been corrected for a missing $1/\pi$ factor;[13] according to later refined calculations by Barma and Subrahmanyam,[34] the quantum-mechanical prediction should have coincide with that of the isotropic model displayed as line FPE2 in Figure 7.] At a first glance, the comparison appears to favor the diffusive model over the isotropic model and hence over the billiard model [the latter two yield identical results in the homogeneous sphere case (see Appendix B)]. However, an inherent inhomogeneous broadening due to different particle sizes inevitably come into play in studies involving ensembles of fine nanoparticles. The inhomogeneous broadening leads to an increased apparent value of ε_2, which may have resulted in a systematic shift of the observed data from the FPE2 line up to FPE1 line in Figure 7 of ref 13.

In the case of nanoshells, experiments have been, as a rule, mostly focused on the range of thin nanoshells with $0.75 \lesssim r_1/r_2 \lesssim 1$, which are most interesting from a practical point of view; they enjoy the largest plasmon red-shift and exhibit the largest field enhancements. This has also been the case of recent experiments on single nanoshells performed by Raschke et al.,[8] wherein the effective mean free path was investigated for individual nanoshells with $r_1 = 15$ nm and with r_2 up to 20 nm. It has been concluded that the best agreement between experiment and theoretical calculations is found for $L_{eff} = D/A$ with $A = 0.5$,[8] that is, for $L_{eff} = 2D$. This behavior for thin shells is exactly that described by the billiard model (see eq 109) without any fitting parameter. Indeed, as shown in Section 6, the thin shell behavior of L_B is, for practical purposes, indistinguishable from its asymptotic $L_B \approx 2D$ for the shell thicknesses of up to $D/R \lesssim 0.3$ (Figure 5). Coincidentally, all the experiments on size-dependent line width broadening in nanoshells[3–5,8,36] appear to be performed for $D/R \lesssim 0.25$ and

hence are within the "linear" range. Note that the billiard, or Lambertian, scattering model appears to be already singled out by the very linear dependence of L_{eff} on D in the thin shell limit, because $L_{\text{eff}} \approx (D/2)\ \ln(2R/D)$ in the diffusive case and $L_{\text{eff}} \approx 14(2RD)^{1/2}/[3\ \ln(2R/D)]$ in the isotropic case (Figure 5). Indeed, all experimental data appear to single out a linear dependence $L_{\text{eff}} = D/A$.[3,4,8]

One can probably explain the previously reported values of $A = 1^3$ and $A = 2 - 3^4$ by a fact that they were found by measurements carried out on nanoshell ensembles, and thus in the presence of an inevitable inhomogeneous broadening. Neglected inhomogeneous distributions of the core/shell ratio may have led to an overestimation of the surface scattering. Later single particle dark field spectroscopy study of larger gold nanoshells with $r_1 \approx 60$ nm and $r_2 \approx 80$ nm by Nehl et al.[36] confirmed that ensemble nanoshell extinction spectra are indeed significantly broadened by particle size and shape inhomogeneity. Furthermore, large A parameters may be caused by rough and incomplete gold shells where electrons may additionally scatter at domain boundaries. Here it is emphasized that, according to the billiard mean free path formula (eq 10), an increase of the enclosure surface at a constant volume naturally leads to a decrease in L_{eff}, that is, a larger effective A. Further, roughness and incompleteness of gold shells may also lead to a lift of the energetic degeneracy of orthogonal plasmon polarizations. This gives rise to an additional contribution to an inhomogeneous broadening of the line width exceeding the inhomogeneity estimated from TEM measurements alone.[8]

For the nanoshells of ref 36, surface scattering corrections should still be feasible (cf eq 1), since the expected mean free path $L_{\text{eff}} \approx 2D = 40$ nm is comparable to $l_\infty = 42$ nm for gold.[13] In spite of that, it has been claimed[36] that for some nanoshells the line width is even narrower than that obtained with the Mie theory calculation without any account of surface scattering corrections. The cause of the narrowing beyond the Mie theory calculation is currently under investigation, but most probably some other effects has become important, such as the segregation of impurities close to the surface,[16] adsorption substrate matrix effects,[16] or faceting of the nanoshell surfaces.[37] Such a narrowing had been reported earlier.[37] In the latter case, the narrowing might be an artifact of the fact that the line width was determined from the scattering cross section and not, as usual, from the absorption cross section.[16] Contrary to some speculations,[16] the electrical charging of metal nanoparticles only shifts the peak position and does not appear to directly influence (only indirectly, via chemisorption)[25] the line width of either spherical particles[25,38] or spheroids.[39] Unless nanoshell can be viewed as a porous aggregation of fine metallic clusters, one can also rule out a structural phase transition, as indicated in the transition from icosehedral to face-centered cubic (fcc) structure in Au clusters.[40] Note additionally that, within the experimentally tested range of $D/R \lesssim 0.25$, one has $L_{\text{i}} > L_{\text{d}} > L_{\text{B}}$ (Figure 5). Therefore, the choice of L_{B} as the mean free path is, even by ignoring its linear asymptotic behavior, still the closest to the reported experimental data (which occasionally indicate an apparent mean free path even smaller than L_{B}) and requires taking into account the minimum of other possible additional broadening mechanisms to fully match experimental data.

7.2 Theoretical and Practical Implications. The most popular choice by far has been, so far, to simply set L_{eff} equal to the shell thickness D.[2–5,8] This choice is expected to yield unrealistically broad homogeneous linewidths. The use of Kachan and Ponyavina[31,32] mean free path L_{KP} (eq 9) does not bring much difference since, for thin shells with $r_1/r_2 \in [0.75, 1)$, one has

$$0.5L_{\text{B}} \le L_{\text{KP}} \lesssim 0.6L_{\text{B}} \tag{120}$$

This is to be expected, because, according to asymptotic (110), $L_{\text{KP}} \approx D$ in the thin shell limit. Therefore, it should only be a negligible difference between using $L_{\text{eff}} = L_{\text{c}} = D$ and $L_{\text{eff}} = L_{\text{KP}}$ for thin shells with $r_1/r_2 \in [0.75, 1)$. For the entire range of shell parameters, one has $L_{\text{B}} \ge (4/3)L_{\text{KP}}$, and the ratio $L_{\text{B}}/L_{\text{KP}}$ monotonically increases from 4/3 for $q = r_1/r_2 = 0$ up to 2 for $q = 1$. Therefore, the normalized total decay rates of the fundamental dipole void-like and sphere-like modes of a gold nanoshell are expected to be significantly less affected by surface scattering than shown in Figure 7 of ref 21. Similarly, the limitations of ref 10 regarding the experimental feasibility of proposed multilabel applications of nanoshells by Chen et al.,[9] which were established on the basis of $L_{\text{eff}} = L_{\text{KP}}$, are expected to become much weaker when $L_{\text{eff}} = L_{\text{B}}$ is to be used.

On comparing the respective asymptotics of L_{GH} and L_B (see eqs 108 and 113) one finds that, approximately (see also Figure 3),

$$\begin{aligned} L_{\text{B}} &< L_{\text{GH}} \quad \text{for} \quad D/R \lesssim 1/4 \\ L_{\text{B}} &> L_{\text{GH}} \quad \text{for} \quad D/R \gtrsim 1/4 \end{aligned} \tag{121}$$

(An exact crossover point is somewhat smaller, namely at 0.23). Consequently, theoretical predictions based on $L_{\text{eff}} = L_{\text{GH}}$ will yield unrealistically narrow line width and the quality factor of the resonance, $Q = E_{\text{res}}/\Gamma$, for thin shells with $D/R \lesssim 1/4$. This has been observed in experiments by Mulvaney and is reported in Section 9 of ref 25.

Schelm and Smith[26,27] took $L_{\text{eff}} = L_{\text{GH}}/4$ as the electron effective mean free path. Because $L_{\text{GH}}/4 < L_{\text{B}}$ over all experimentally feasible range of nanoshell parameters, the limits of Schelm and Smith[27] on resonance tunability in metallic nanoshells can be probably somewhat relaxed, since they were established on assuming too large line width broadening. For the same reasons, actual internal electric field densities in and around metal nanoshells are expected to be somewhat larger than predicted.[26]

8. Conclusions

The widely adopted practice that the electron effective mean free path L_{eff} for thin shells is, irrespective of the underlying surface scattering model, proportional to the shell thickness D,[2–5,8] has to be abandoned. Qualitatively different nonlinear dependences on the inner and outer shell radii result for different model cases in the shell geometry. This has been confirmed by calculating the mean free path for the shell geometry under the assumptions of (i) diffusive, (ii) isotropic, and (iii) billiard, or Lambertian, scattering.

A comparison with preliminary experimental results on individual core−shell particles appears to indicate that only the billiard, or Lambertian, scattering model is compatible with both the homogeneous sphere and spherical shell case. (The model predictions are also compatible with recent experiments on homogeneous gold nanorods.[41]) The success of the Euler diffusive scattering in the homogeneous sphere case[11–14] seems to be purely accidental, because all the scattering models yield a linear dependence of the mean free path on the sphere radius with minor differences in the proportionality factor. A fact that the mean free path in the shell geometry is much more sensitive to underlying model assumptions of electron surface scattering can be used in future experiments on single and well-controlled

dielectric core-metal shell nanoparticles (preferably with a constant total radius R and variable D) in order to test theoretical predictions for the full range of nanoparticle parameters, and in particular for $D/R \lesssim 0.3$, that is, outside the "linear" range, in which case deviations from the linear behavior $L_{\text{eff}} = 2D$ should become transparent (Figure 5) and thereby discriminate between different surface scattering models. This would enable one to more precisely assess the contribution of other mechanisms, such as chemical interface damping, to overall plasmon resonance damping. It would be also interesting to perform quantum-mechanical calculations in the shell geometry for the full range of shell parameters. This will be dealt with elsewhere.

Appendix

A

Summary of Elementary Formulas

The law of cosines (also known as the cosine formula or cosine rule),

$$c^2 = a^2 + b^2 - 2ab\cos\theta \tag{122}$$

where θ is the angle between the sides a and b of a triangle and c is the remaining side opposing the angle.

$$\int_a^b \cos\theta \sin\theta \, \mathrm{d}\theta = \int_{\cos b}^{\cos a} x \, \mathrm{d}x = \frac{\cos^2 a - \cos^2 b}{2} \tag{123}$$

$$\int_a^b \cos^2\theta \sin\theta \, \mathrm{d}\theta = \int_{\cos b}^{\cos a} x^2 \, \mathrm{d}x = \frac{\cos^3 a - \cos^3 b}{3} \tag{124}$$

$$\int \sqrt{y^2 - 1} \, \mathrm{d}y = \frac{1}{2}\left(y\sqrt{y^2 - 1} - \ln\left|y + \sqrt{y^2 - 1}\right|\right) \tag{125}$$

$$\int \frac{x \, \mathrm{d}x}{x - a} = x + a\ln|x - a| \tag{126}$$

$$\int \frac{\mathrm{d}x}{(x - a)(b - x)} = \frac{1}{b - a}\ln\left|\frac{x - a}{b - x}\right| \tag{127}$$

$$\int \frac{x^2 \, \mathrm{d}x}{(x - a)(b - x)} = -x - \frac{1}{b - a}[b^2 \ln|b - x| - a^2 \ln|x - a|] \tag{128}$$

$$\int \frac{x \, \mathrm{d}x}{\sqrt{b - x}} = -\frac{2}{3}(2b + x)\sqrt{b - x} \tag{129}$$

$$\int \frac{\mathrm{d}x}{(b - x)^{3/2}} = \frac{2}{\sqrt{b - x}} \tag{130}$$

$$\frac{x^2 \, \mathrm{d}x}{(b - x)^{3/2}} = \left[-\frac{(b - x)^2}{3} + 2b(b - x) + b^2\right]\frac{2}{\sqrt{b - x}} = -\frac{2}{3}(b - x)^{3/2} + 4b\sqrt{b - x} + \frac{2b^2}{\sqrt{b - x}} \tag{131}$$

Here eq 126 is given as eq 1.2.4.13 by ref 42 and can also be easily verified by differentiation. The identity 127 is given as eq 1.2.7.7 by ref 42 and results from the elementary identity

$$\frac{1}{(x + a)(x + b)} = \frac{1}{b - a}\left(\frac{1}{x + b} - \frac{1}{x + a}\right) \tag{132}$$

The identity 128 is given as eq 1.2.7.9 by ref 42 and results from the elementary identity

$$\frac{1}{(x + a)(x + b)} = 1 + \frac{1}{a - b}\left(\frac{b^2}{x + b} - \frac{a^2}{x + a}\right) \tag{133}$$

The identities 129–131 can be derived using eqs 1.2.18.6, 1.2.18.9, and 1.2.18.11 of ref 42.

Regarding the thin-shell limit $r_1 \to r_2$, the following expressions have been repeatedly used:

$$r_1 + r_2 = 2R - D \tag{134}$$

$$q = 1 - \frac{D}{R} \tag{135}$$

$$q^2 = \frac{(R - D)^2}{R^2} = 1 - \frac{2D}{R} + \frac{D^2}{R^2} \tag{136}$$

$$\frac{1}{1 + q^2} \approx \frac{1}{2}\left(1 + \frac{D}{R} + \frac{D^2}{2R^2}\right) \tag{137}$$

$$\frac{1}{r_1} = \frac{1}{R - D} \approx \frac{1}{R}\left(1 + \frac{D}{R}\right) \tag{138}$$

which follow upon writing $r_1 = R - D$.

B

Homogeneous Sphere

Upon applying the law of cosines (eq 122), one finds for the sphere chord length (cf eq 87)

$$L(\theta) = 2R\cos\theta \tag{139}$$

Upon integrating $L(\theta)$ with the respective probability measures, eqs 28, 29, and 31, the following mean free paths in the case of a homogeneous sphere with radius R are obtained:

•In the diffusive case,

$$L_{\text{d}} = R \tag{140}$$

i.e., the effective mean free path of the conduction electrons is equal to the homogeneous sphere radius.[11]

•In the isotropic and billiard cases,[13,29]

$$L_{\text{i}} = L_{\text{B}} = 4R/3 \tag{141}$$

The result for L_{d} follows upon using eq 123, whereas that for L_{i} and L_{B} follows on using eq 124. Note in passing that the equality $L_{\text{i}} = L_{\text{B}}$ in the homogeneous sphere case follows from the equality $\mathrm{d}\mu_{\text{i}} = \mathrm{d}\mu_{\text{B}}$, which in turn follows upon substituting eq 139 into eq 29 together with $c_{\text{i}} = 1/L_{\text{d}} = 1/R$.

Thus, as established earlier,[11–14] the mean free-path in the homogeneous sphere case is always linearly proportional to the sphere radius R, irrespective of the assumptions regarding the electron surface scattering.

Acknowledgment. I thank Professors Chernov, Klar, and Mulvaney for discussion.

Supporting Information Available: Intermediary calculation steps are supplied together with the wording of the Birkhoff-Khinchin theorem and an amenable derivation of the billiard formula in its general form (eq 10). This material is available free of charge via the Internet at http://pubs.acs.org.

References and Notes

(1) Neeves, A. E.; Birnboim, M. H. J. *Opt. Soc. Am. B* **1989**, *6*, 787.
(2) Zhou, H. S.; Honma, I.; Komiyama, H.; Haus, J. W. *Phys. Rev. B* **1994**, *50*, 12052.
(3) Averitt, R. D.; Sarkar, D.; Halas, N. J. *Phys. Rev. Lett.* **1997**, *78*, 4217.
(4) Westcott, S. L.; Jackson, J. B.; Radloff, C.; Halas, N. J. *Phys. Rev. B* **2002**, *66*, 155431.
(5) Grady, N. K.; Halas, N. J.; Nordlander, P. *Chem. Phys. Lett.* **2004**, *399*, 167.
(6) Hirsch, L. R.; Stafford, R. J.; Bankson, J. A.; Sershen, S. R.; Rivera, B.; Price, R. E.; Hazle, J. D.; Halas, N. J.; West, J. L. *Proc. Natl. Acad. Sci. U.S.A.* **2003**, *100*, 13549.

(7) Loo, C.; Hirsch, L.; Lee, Min-Ho.; Chang, E.; West, J.; Halas, N. J.; Drezek, R. *Opt. Lett.* **2005**, *30*, 1012.
(8) Raschke, G.; Brogl, S.; Susha, A. S.; Rogach, A. L.; Klar, T. A.; Feldmann, J.; Fieres, B.; Petkov, N.; Bein, T.; Nichtl, A.; Kürzinger, K. *Nano Lett.* **2004**, *4*, 1853.
(9) Chen, K.; Liu, Y.; Ameer, G.; Backman, V. J. *Biomed. Opt.* **2005**, *10*, 024005.
(10) Khlebtsov, B.; Khlebtsov, N. J. *Biomed. Opt.* **2006**, *11*, 044002.
(11) Euler, J. Z. *Phys.* **1954**, *137*, 318.
(12) Kreibig, U.; Fragstein, C. V. Z. *Phys. A* **1969**, *224*, 307.
(13) Kreibig, U. J. *Phys. F: Met. Phys.* **1974**, *4*, 999.
(14) Kreibig, U.; Genzel, L. *Surf. Sci.* **1985**, *156*, 678.
(15) Hövel, H.; Fritz, S.; Hilger, A.; Kreibig, U.; Vollmer, M. *Phys. Rev. B* **1993**, *48*, 18178.
(16) Kreibig, U.; Vollmer, M. *Optical Properties of Metal Clusters*, Springer Series in Materials Science; Springer: Berlin, 1995.
(17) Bohren C. F.; Huffman, D. R. *Absorption and Scattering of Light by Small Particles*; John Wiley & Sons: New York, 1998.
(18) Kraus, W. A.; Schatz, G. C. J. *Chem. Phys.* **1983**, *79*, 6130.
(19) Reynolds, F. W.; Stilwell, G. R. *Phys. Rev.* **1952**, *88*, 418.
(20) Klar, T.; Perner, M.; Grosse, S.; von Plessen, G.; Spirkl, W.; Feldmann, J. *Phys. Rev. Lett.* **1998**, *80*, 4249.
(21) Teperik, T. V.; Popov, V. V.; García, de.; Abajo, F. J. *Phys. Rev. B* **2004**, *69*, 155402.
(22) Sander, L. *J. Phys. Chem. Solids* **1968**, *29*, 291. As noticed by Ruppin and Yatom,[23] eq 19 should be corrected by a factor of 1/2.
(23) Ruppin, R.; Yatom, H. *Phys. Status Solidi B* **1976**, *74*, 647.
(24) Granqvist, C. G.; Hunderi, O. Z. *Phys. B* **1978**, *30*, 47.
(25) Mulvaney, P. *Langmuir* **1996**, *12*, 788.
(26) Schelm, S.; Smith, G. B. J. *Phys. Chem. B* **2005**, *109*, 1689.
(27) Schelm, S.; Smith, G. B. J. *Opt. Soc. Am. A* **2005**, *22*, 1288.
(28) Xu, Hongxing. *Phys. Rev. B* **2005**, *72*, 073405.
(29) Chernov, N. J. *Stat. Phys.* **1997**, *88*, 1.
(30) Chernov, N.; Markarian, R. *Introduction to the Ergodic Theory of Chaotic Billiards*; http://www.math.uab.edu/chernov/papers/rbook.pdf.
(31) Kachan, S. M.; Ponyavina, A. N. *Physics, Chemistry and Application of Nanostructures: Reviews and Short Notes to Nanomeeting 1999*, Minsk, Belarus, May 17−21, 1999; World Scientific: Singapore, 1999; p. 103.
(32) Kachan, S. M.; Ponyavina, A. N. J. *Mol. Struct.* **2001**, *563−564*, 267.
(33) Coronado, E. A.; Schatz, G. C. J. *Chem. Phys.* **2003**, *119*, 3926.
(34) Barma, M.; Subrahmanyam, V. J. *Phys.: Condens. Matter* **1989**, *1*, 7681.
(35) Kawabata, A.; Kubo, R. J. *Phys. Soc. Japan* **1966**, *21*, 1765. There should be a factor of $1/\pi^3$ in the resulting expressions (4.12) for $\varepsilon_2(\omega)$; cf. eq 10 of ref 13.
(36) Nehl, C. L.; Grady, N. K.; Goodrich, G. P.; Tam, F.; Halas, N. J.; Hafner, J. H. *Nano Lett.* **2004**, *4*, 2355.
(37) Sönnichsen, C.; Franzl, T.; Wilk, T.; von Plessen, G.; Feldmann, J. *New J. Phys.* **2002**, *4*, 93–1.
(38) Rostalski, J.; Quinten, M. *Colloid Polym. Sci.* **1996**, *274*, 648.
(39) Mulvaney, P.; Pérez-Juste, J.; Giersig, M.; Liz-Marzán, L. M.; Pecharromán, C. *Plasmonics* **2006**, *1*, 61.
(40) Kreibig, U. *Solid State Commun.* **1978**, *28*, 767.
(41) Novo, C.; Gomez, D.; Pérez-Juste, J.; Zhang, Z.; Petrova, H.; Reismann, M.; Mulvaney, P.; Hartland, G. V. *Phys. Chem. Chem. Phys.* **2006**, *8*, 3540.
(42) Prudnikov, A. P.; Brychkov, Yu. A. Marichev, O. I. *Integrals and Series*, 2nd ed; Gordon and Breach: London, 1988.

JP8010074